# A single-cell view on the ecophysiology of anaerobic phototrophic bacteria

Niculina Musat[a,1], Hannah Halm[a], Bärbel Winterholler[b], Peter Hoppe[b], Sandro Peduzzi[c], Francois Hillion[d], Francois Horreard[d], Rudolf Amann[a], Bo B. Jørgensen[a], and Marcel M. M. Kuypers[a]

[a]Max Planck Institute for Marine Microbiology, Celsiusstrasse 1, 28359 Bremen, Germany; [b]Max Planck Institute for Chemistry, Johann-Joachim-Becher Weg 27, 55128 Mainz, Germany; [c]Cantonal Institute of Microbiology and Alpine Biology Center Foundation Piora, Via Mirasole 22A, CH-6500 Bellinzona, Switzerland; and [d]Cameca, Quai des Gresillons 29, 92622 Gennevilliers Cedex, France

Quantitative information on the ecophysiology of individual microorganisms is generally limited because it is difficult to assign specific metabolic activities to identified single cells. Here, we develop and apply a method, Halogen In Situ Hybridization-Secondary Ion Mass Spectroscopy (HISH-SIMS), and show that it allows simultaneous phylogenetic identification and quantitation of metabolic activities of single microbial cells in the environment. Using HISH-SIMS, individual cells of the anaerobic, phototropic bacteria *Chromatium okenii*, *Lamprocystis purpurea*, and *Chlorobium clathratiforme* inhabiting the oligotrophic, meromictic Lake Cadagno were analyzed with respect to $H^{13}CO_3^-$ and $^{15}NH_4^+$ assimilation. Metabolic rates were found to vary greatly between individual cells of the same species, showing that microbial populations in the environment are heterogeneous, being comprised of physiologically distinct individuals. Furthermore, *C. okenii*, the least abundant species representing ≈0.3% of the total cell number, contributed more than 40% of the total uptake of ammonium and 70% of the total uptake of carbon in the system, thereby emphasizing that numerically inconspicuous microbes can play a significant role in the nitrogen and carbon cycles in the environment. By introducing this quantification method for the ecophysiological roles of individual cells, our study opens a variety of possibilities of research in environmental microbiology, especially by increasing the ability to examine the ecophysiological roles of individual cells, including those of less abundant and less active microbes, and by the capacity to track not only nitrogen and carbon but also phosphorus, sulfur, and other biological element flows within microbial communities.

anaerobic phototrophs | nanoSIMS

**M**olecular biological approaches have in recent years provided a wealth of high-resolution information regarding the genetics, ecology, and evolution of microbial populations (1–5). At the cellular level, however, quantitative information on the ecophysiology of individual microorganisms in the environment is generally scarce (see refs. 6 and 7). A major goal, therefore, is to assign specific metabolic activities to the identities of individual cells. A particularly promising approach to this objective is Secondary Ion Mass Spectrometry (SIMS), which was applied for the first time in environmental microbiology to follow inorganic carbon and nitrogen assimilation by bacterial and fungal cells and to show that aggregates of archaea and sulfate-reducing bacteria founds in sediments where anaerobic oxidation of methane predominated were indeed consuming methane (6, 8). Single-cell resolution with sufficient mass-resolving power was, however, only recently achieved through the development of nano-scale secondary-ion mass spectrometry (nanoSIMS). Other methods currently used either do not provide single-cell resolution or, like microautoradiography, require that microorganisms be fed radioactively labeled substrates. The uptake of radioisotopes then directly links individual microbial cells to their activity in the environment (ref. 7 and references therein). However, this approach is limited to elements that have a radioisotope with a suitable half-life (>1 d; for example

$^{14}C$ and $^3H$) and excludes the study of other elements such as nitrogen. NanoSIMS, on the other hand, can be used to measure the distribution of any stable isotope as well as any radioisotope with a suitable half-life, and thus, the uptake of radioactive or stable-isotope labeled substrates can be monitored (9). Using nanoSIMS, carbon and nitrogen uptake by nitrogen-fixing cyanobacteria (10) and in situ nitrogen fixation by individual bacterial symbionts of shipworms (11) have been quantified. When combined with in situ hybridization using halogen- or stable-isotope-labeled gene probes, nanoSIMS can additionally be used for the identification of individual microbes (12, 13).

Here we developed and applied a method that allowed us to examine the ecophysiology of single cells in the environment using nanoSIMS. It uses horseradish-peroxidase-labeled oligonucleotide probes and fluorine-containing tyramides for the identification of microorganisms in combination with stable-isotope-labeling experiments for analyzing the metabolic function of single microbial cells. Using this method, we have quantified metabolic activities of single cells of purple and green sulfur bacteria inhabiting the oligotrophic, meromictic Lake Cadagno, a stratified alpine lake located in the Piora Valley in the Southern Alps of Switzerland. Springs supply salty water to its depths (14), and, as a result, Lake Cadagno is permanently stratified. The upper, oxic waters are well-mixed and contain low concentrations of phosphate and nitrate (14, 15). The anoxic, lower layer is stagnant and enriched in phosphate and ammonium. At the chemocline between these 2 layers, sharp gradients appear in depth profiles of these nutrients and in those of oxygen, sulfate, sulfide, and light (14, 16).

The physicochemical conditions favor development at the chemocline of a community consisting mainly of purple and green photosynthetic sulfur bacteria. The seasonal variations of this assemblage have been studied intensively in the past 10 years (15–17) and make this lake an attractive test system for investigating the activities of single cells. These anaerobic phototrophs, which use light energy to oxidize sulfide and other reduced sulfur compounds, are commonly found in seasonally or permanently stratified lakes, anoxic ponds or sediments. Numerically abundant, in many of these environments they are responsible for the oxidation of the entire sulfide flux and thus play a critical role in the sulfur cycle (18–20). However, the distribution of processes and materials among individual cells in such environments remains unknown.

Here we quantified and compared ammonium and inorganic carbon uptake of 3 species of anaerobic phototrophs, *Chlorobium*

---

ENVIRONMENTAL SCIENCES

**Fig. 1.** Vertical distribution of turbidity, oxygen, total cell numbers, and relative abundance of *C. clathratiforme*, *C. okenii*, and *L. purpurea* (*A*), temperature and conductivity (*B*), and redox potential and inorganic nitrogen (*C*).

*clathratiforme*, *Chromatium okenii*, and *Lamprocystis purpurea*, and quantitatively determined their contribution to the total ammonium and inorganic carbon assimilation in the system. Moreover, metabolic activities of individual cells belonging to the same species were analyzed and compared. We conclude that halogen in situ hybridization coupled to secondary ion mass spectrometry (HISH-SIMS) will provide hitherto unavailable information about microbial populations.

## Results and Discussion

**Physicochemical Parameters of Lake Cadagno and Relative Abundance of Anaerobic Phototrophs.** Measurements of physicochemical parameters confirmed earlier reports (16, 21, 22), showing steep vertical gradients of nutrients and oxygen within the pycnocline and a shift in redox potential between 10- and 11-m depth, indicating anoxic, reducing conditions in the hypolimnion (Fig. 1). A turbidity maximum was identified at 11.7-m depth, coinciding with a dense microbial community, amounting to $2.1 \times 10^7$ cells mL$^{-1}$, which mainly consisted of green and purple sulfur bacteria (Fig. 1). Based on these measurements, 3 depths (10.5, 11.5, and 12.5 m) spanning the chemocline were chosen for sampling and for further analyses of the phototrophic sulfur bacterial community. The most abundant microorganism at those depths was the green sulfur bacterium, *C. clathratiforme*, amounting to $1.7 \times 10^7$ cells mL$^{-1}$ [Figs. 1 and 2 and supporting information (SI) Table S1]. Purple sulfur bacteria *L. purpurea* and *C. okenii* were detected in much lower numbers, of $1.1–2.9 \times 10^5$ cells mL$^{-1}$ and $4.4–8.4 \times 10^4$ cells mL$^{-1}$, respectively (Figs. 1 and 2 and Table S1). Other anaerobic phototrophs present were *Lamprocystis roseopersicina* and *Chlorobium phaeobacteroides*, amounting to $2.7 \times 10^5$ cells mL$^{-1}$ and $5.1 \times 10^4$ cells mL$^{-1}$, respectively (Table S1). These results confirmed previous studies (17, 22) describing a numerically stable phototrophic community strongly dominated by *C. chlatratiforme*.

**Single-Cell Analysis.** We analyzed single cells of *C. clathratiforme*, the most abundant microorganism at all depths investigated, *L. purpurea*, one of the most abundant, small-celled, purple sulfur bacteria, and *C. okenii*, the only large-celled purple sulfur bacterium present. For this purpose, water samples from 11.5-m depth were incubated for 12 h at in situ light and temperature conditions after addition of $^{15}$N-labeled ammonium and $^{13}$C-labeled bicarbonate. After incubation, the samples were handled as described for *Escherichia coli* and *Azoarcus* sp. cells (*SI Text*) and hybridized with HRP-labeled oligonucleotide probes targeting specific regions of the 16S rRNA of the 3 species.

After the deposition of fluorine-containing tyramides, filters were immediately analyzed using nanoSIMS. For each individual cell, we recorded simultaneously secondary-ion images of naturally abundant $^{12}$C (measured as $^{12}$C$^-$) and $^{14}$N (measured as $^{12}$C$^{14}$N$^-$) atoms and, similarly, of $^{13}$C, $^{15}$N, and $^{19}$F (Figs. 3–5). Regions of interest around individual cells or clusters of cells were defined by using the $^{19}$F signal as a mask. For each region of interest, $^{15}$N/$^{14}$N (inferred from the $^{12}$C$^{15}$N/$^{12}$C$^{14}$N ratio) and $^{13}$C/$^{12}$C ratios were calculated and compared with the natural abundance ratios (Table S2).

All analyzed cells were substantially enriched in $^{15}$N and $^{13}$C relative to the nonamended cells (Figs. 3–5 and Table S2). There were significant differences in $^{15}$N/$^{14}$N and $^{13}$C/$^{12}$C ratios between species, with *C. okenii* having the highest isotopic enrichments followed by *L. purpurea* and *C. clathratiforme* (Figs. 3–5 and Table S2). Moreover, large differences in $^{15}$N/$^{14}$N and $^{13}$C/$^{12}$C ratios were observed between individual cells of the same species, reflecting obvious differences in metabolic status or different types of metabolism (see *C, D, G,* and *H* of Figs. 3–5). Unexpectedly, even cells that were attached to each other (e.g., *C. clathratiforme* cells within the same filament) had very different $^{15}$N/$^{14}$N and $^{13}$C/$^{12}$C ratios (see marked cells and arrows in Fig. *3 C, D, G,* and *H* and Table S2,
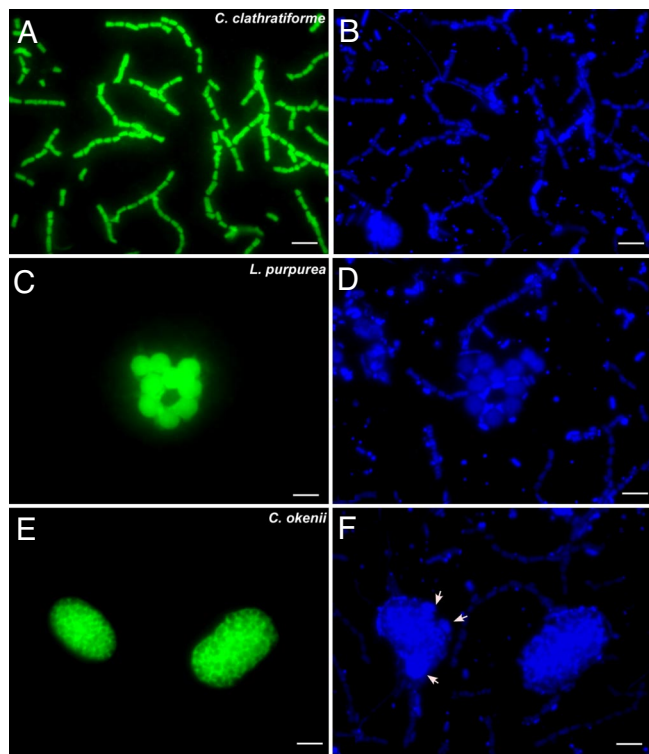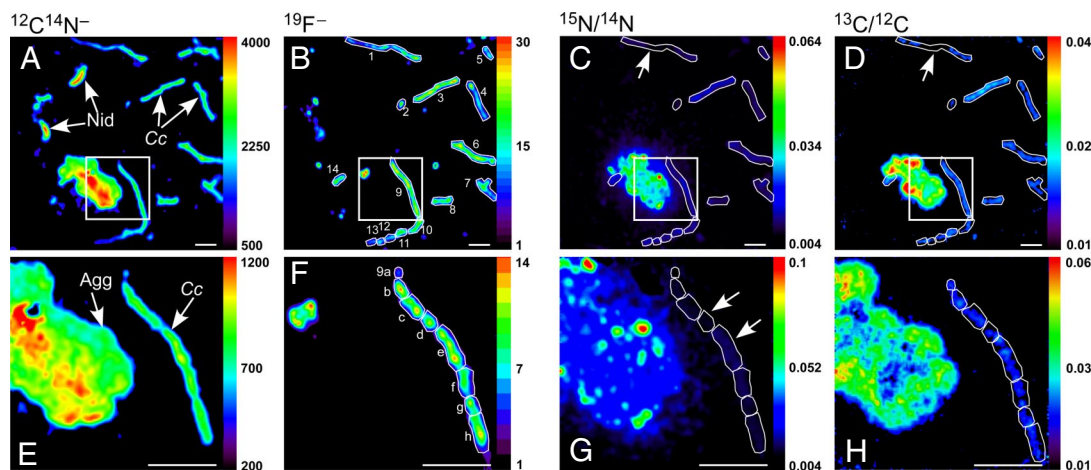
**Fig. 2.** Epifluorescence micrographs of purple and green sulfur bacteria hybridized with species-specific HRP-oligonucleotide probes for the 3 species and fluorine-containing tyramides (*A*, *C*, and *E*). Corresponding fields stained with DAPI show all cells in blue (*B*, *D*, and *F*). Arrows in *F* indicate epibionts attached to *C. okenii*. (Scale bars, 5 $\mu$m.)

same ranges were approximately 2-fold and 2-fold. For *C. okenii* they were approximately 7-fold and 3-fold (Fig. 6*A*). Nonetheless, cells belonging to the same species generally grouped together in three distinct clusters based on ammonium and inorganic carbon assimilation (Fig. 6*A*).

A notable exception was one particular *C. okenii* cell that had epibiontic microorganisms attached to the surface and that was characterized by significantly lower ammonium uptake than other *C. okenii* cells (Figs. 5*C* and 6*A*). This association with epibiontic cells is not unique. In fact, a substantial proportion of the *C. okenii* cells observed with fluorescence microscopy had similar epibiontic cells attached (e.g., Fig. 2*F*). Such epibionts growing on *Chromatium* species have been previously observed and it has been suggested that these organisms could be either parasitic or opportunistic bacteria growing on dissolved organic matter excreted by the host cells (23, 24). Although the analysis of a single cell does not allow us to determine the nature of the association between *C. okenii* and the epibionts, it illustrates that HISH-SIMS can visualize interactions between individual microbes in microbial aggregates in an unparalleled way. In a similar approach, the function of individual members of microbial consortia, microbial mats, and biofilms could be studied using HISH-SIMS.

By averaging and comparing the uptake rates of individual cells of each species, we determined that the least abundant *C. okenii* assimilated approximately 60 times more ammonium and 70 times more inorganic carbon than *L. purpurea* and approximately 700 times more ammonium and 1,000 times more inorganic carbon than *C. clathratiforme* in the chemocline of Lake Cadagno (Fig. 6*A*). These large differences can partly be explained by differences in cell volume between species. When normalized to cell volume, the differences between the 3 species became smaller but were still substantial (Fig. S1). *C. okenii* assimilated on average approximately 2 times more carbon per $\mu$m$^3$ of biomass than *L. purpurea* and 3 times more ammonium and 5 times more carbon than *C. clathratiforme*. The calculated average atomic C:N ratio (9.1) for in situ inorganic carbon and ammonium assimilation for *C. clathratiforme* was lower than the C:N ratio (11.1) for in situ assimilation by *L. purpurea* cells (Fig. 6*A*). Uptake by *C. okenii* cells was characterized by high uptake C:N values (on average 14.8) (Fig. 6*A*). For all 3 species, the C:N ratios substantially exceeded the Redfield value (6.6) (25), which could indicate that these organisms accumulate carbon-rich storage compounds [e.g., glycogen, starch, or polyhydroxyalkanoates] in large quantities within the cell (26).

cells 3*F* 9*a–h*). These differences were even more evident when cell-specific uptakes of ammonium and dissolved inorganic carbon were calculated by using the $^{15}$N/$^{14}$N and $^{13}$C/$^{12}$C ratios and the volumes per cell determined for each species (Fig. 6*A* and Table S2). The volume estimates for *C. clathratiforme*, *L. purpurea*, and *C. okenii* were 1.2, 5.3, and 270 $\mu$m$^3$ per cell, respectively. Uptakes of ammonium and of inorganic carbon by individual cells of *C. clathratiforme* varied significantly. The range was approximately 12-fold for ammonium and 7-fold for carbon. For *L. purpurea* the
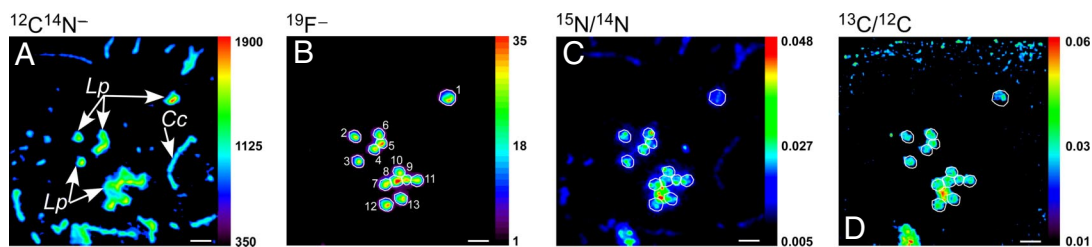


**Fig. 3.** $^{15}$N-ammonium and $^{13}$C-inorganic carbon uptake by individual *C. clathratiforme* cells. Parallel secondary ion images of *C. clathratiforme* cells (Cc), not identified microbes (Nid) (*A–D*), and of an aggregate of not identified bacteria (Agg) (*E–H*). The square represents a 15×15-$\mu$m field chosen for further sputtering. The abundances of $^{12}$C$^{14}$N$^-$ (*A* and *E*), $^{19}$F$^-$ (*B* and *F*), and the $^{15}$N/$^{14}$N (*C* and *G*) and $^{13}$C/$^{12}$C (*D* and *H*) ratios are shown. The numbers and markings around cells in figure define regions of interest which were used for calculation of $^{15}$N/$^{14}$N and $^{13}$C/$^{12}$C ratios (see Table 3). (Scale bars, 5 $\mu$m.)
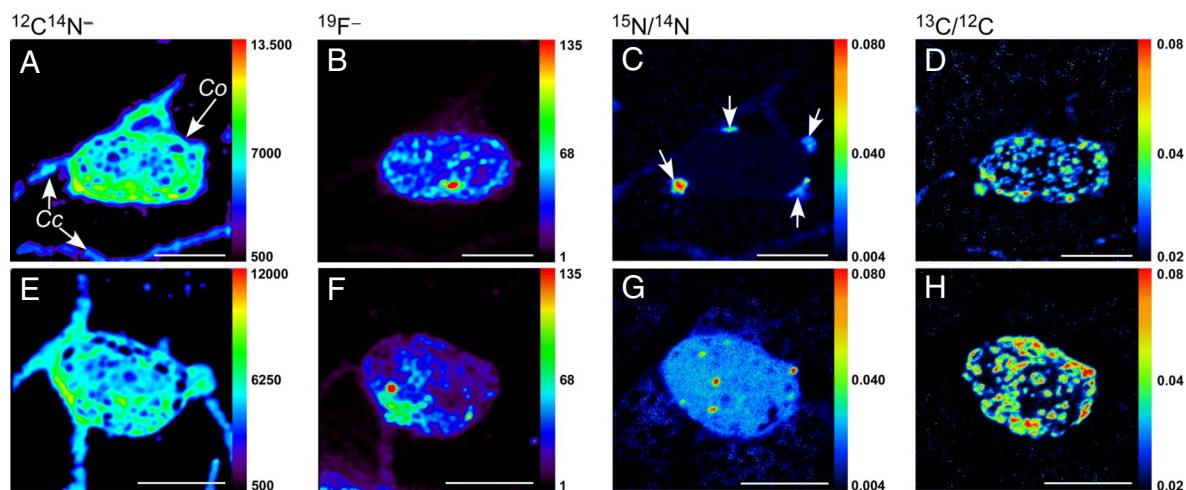
**Fig. 4.** ¹⁵N-ammonium and ¹³C-inorganic carbon uptake by individual *L. purpurea* cells. Parallel secondary ion images of *L. purpurea* cells (*Lp*) and presumably *C. clathratiforme* cells (*Cc*) (*A–D*). The abundances of $^{12}C^{14}N^-$ (*A*), $^{19}F^-$ (*B*), and the $^{15}N/^{14}N$ (*C*) and $^{13}C/^{12}C$ (*D*) ratios are shown. The numbers and markings around cells are defined in the legend of Fig. 4. (Scale bars, 5 $\mu$m.)

Based on $^{15}N/^{14}N$ and $^{13}C/^{12}C$ ratios of individual cells and on the labeling percentages of the substrates used (i.e., $H^{13}CO_3^-$ and $^{15}NH_4^+$), we calculated the doubling times for *C. okenii*, *L. purpurea*, and *C. clathratiforme* cells. We assumed that all carbon and ammonium assimilated stimulated growth of new cells. This supposition can lead to an underestimation of the carbon-based doubling times for species that deposit C-rich storage compounds (20). For all 3 species, particularly *C. clathratiforme*, C-based doubling times varied widely (Fig. 7). Moreover, large differences were observed between *C. okenii* and *L. purpurea* species, with average, C-based doubling times of 5 and 7 days, and *C. clathratiforme*, with average doubling times of 36 days (Fig. 7). For *L. purpurea*, and *C. okenii* the average N-based doubling times were in good agreement with the C-based doubling times (Fig. 7). In contrast, the average N-based doubling time for *C. clathratiforme* (45 days) substantially exceeded the C-based growth rates, indicating that this anaerobic phototroph may indeed deposit C-rich storage products. The observed doubling times for all 3 species were significantly longer than those (0.5–1.5 days) reported for pure cultures of green and purple sulfur bacteria grown under ideal laboratory conditions (27–29) but were within the range (0.3–125 d) (20) of doubling times estimated from bulk in situ measurements of biomass or $CO_2$ fixation (20, 30, 31). Intriguingly, the C-and N-based doubling times (7 and 8 days) for bulk biomass from the Lake Cadagno chemocline were comparable with the doubling times for *C. okenii* and *L. purpurea* and substantially shorter than the doubling time for *C. clathratiforme* (Fig. 7), indicating that the most abundant species (i.e., *C. clathratiforme*) was not the main contributor to total ammonium and inorganic carbon assimilation.

We determined the total uptake of ammonium and inorganic carbon for each species by multiplying the average uptake rates by the absolute cell abundance. Summed, these accounted for ≈57% of total ammonium uptake and ≈85% of total inorganic carbon uptake in the system as measured by bulk incubations and analyses (Figs. 6 *B* and *C*). *C. okenii* with a total biovolume of $1.8 \times 10^7$ $\mu$m³ mL⁻¹ contributed approximately 40% to the total ammonium uptake and 70% to the inorganic carbon uptake. In contrast, *C. clathratiforme* with a slightly larger total biovolume ($2.1 \times 10^7$ $\mu$m³ mL⁻¹) contributed only approximately 15% and 15% to the total uptakes of ammonium and inorganic carbon, respectively. *L. purpurea*, with the smallest total biovolume ($6.9 \times 10^5$ $\mu$m³ mL⁻¹), contributed the least, with uptakes of ammonium and inorganic carbon accounting for 1.3% and 1.6% of the totals, respectively. These results confirm that *C. clathratiforme*, by far the most abundant species and having the highest biovolume, was not the main assimilator of ammonium and inorganic carbon. Even more puzzling was the low abundance of *C. okenii*, which represented a very small fraction (<1% of the total cell number) of the microbial community within the chemocline.

At present, we can only speculate why an organism with an average doubling time 7 times shorter than *C. clathratiforme* is present in such low abundance. The relative abundance of these species might have been influenced by an enhanced predation pressure in the system. *C. okenii* could have been subjected to a higher predation pressure by anaerobic protozoa and predatory prokaryotes (23, 32). Growing in net-like structures or large aggregates, *C. clathratiforme* and *L. purpurea* are less susceptible to protozoan grazers than are the single cells of *C. okenii* (33, 34). On the other hand, growth as single, motile cells provides an advantage to *C. okenii*, which can move freely through the water column and



**Fig. 5.** ¹⁵N-ammonium and ¹³C-inorganic carbon uptake by individual *C. okenii* cells. Parallel secondary ion images of *C. okenii* cells (*Co*) and presumably *C. clathratiforme* cells (*Cc*) (*A–H*). The abundances of $^{12}C^{14}N^-$ (*A* and *E*), $^{19}F^-$ (*B* and *F*), and the $^{15}N/^{14}N$ (*C* and *G*) and $^{13}C/^{12}C$ (*D* and *H*) ratios are shown. Arrows in *C* indicate highly active epibionts attached to a *C. okenii* cell. The numbers and markings around cells are defined in the legend of Fig. 4. (Scale bars, 5 $\mu$m.)
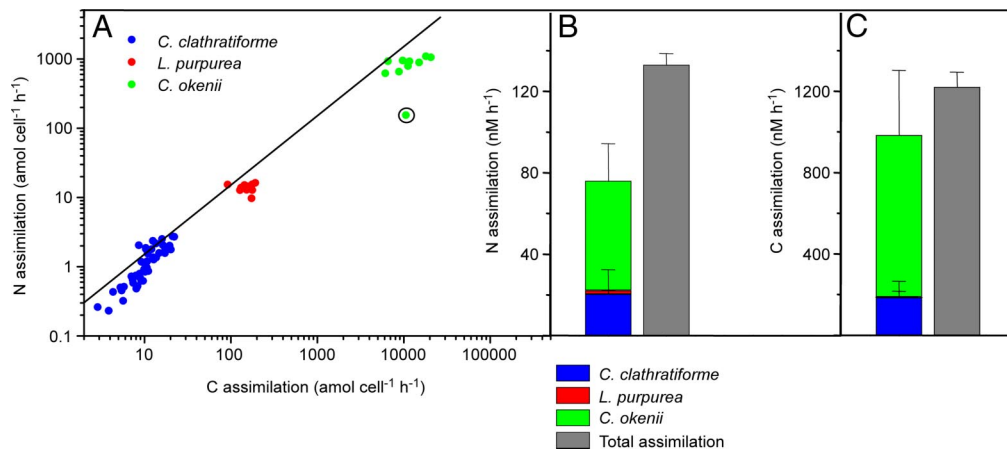
**Fig. 6.** Ammonium and inorganic carbon assimilation by green and purple sulfur bacteria in Lake Cadgno. Ammonium versus inorganic carbon uptake by individual *C. clathratiforme*, *L. purpurea*, and *C. okenii* cells (*A*). The line represents the theoretical 'Redfield', C:N ratio of 6.6. Contribution to the total ammonium (*B*), and total dissolved inorganic carbon (*C*) assimilation in the system by each population. For the calculation of total nitrogen and carbon uptake, the absolute abundance of each species as determined by CARD-FISH was taken into account.

find the best zones of nutrient availability and light intensity for its metabolic requirements.

One of the most intriguing findings in our study was the large range of uptake rates of ammonium and inorganic carbon for single cells of the same species (Fig. 6*A* and Table S2). These substantial differences could be the result of genomic diversity in phylogenetically identical (or closely related) but physiologically distinct populations (35, 36). In recent years, molecular techniques have revealed remarkable genetic and physiological diversity among microorganisms of the same sample species (2, 4, 36, 37). The genetic heterogeneity could be the basis for a physiological diversity that provides selective advantages to different genotypes under changing conditions (38). In the chemocline of Lake Cadagno, the populations of anaerobic phototrophs can benefit greatly from a continuous selection of the fittest subpopulations under changes of nutrient concentrations, light intensity, or redox conditions. Such genotypic plasticity may be advantageous especially for nonmotile species such as *C. clathratiforme*, which are not capable of actively moving through the chemocline to find the optimal growth conditions in a variable environment.

An alternative explanation for the high metabolic variability of individual cells within the same species could be nongenetic heterogeneity caused by differences in gene expression among individual bacteria (39). Cells of different age or with different life histories would be in different physiological states. They might have experienced different ammonium or sulfide concentrations, have suffered from traces of oxygen, or adapted to different light intensities. Although this hypothesis could be tested by monitoring specific mRNA in single cells of a 16S rRNA-defined population (40), a proof of genomic heterogeneity would still require population-genetic studies of isolates or metagenomic studies.

In conclusion, by applying HISH-SIMS to green and purple sulfur bacteria from a natural environment, we found a remarkable variability in metabolic rates of individual cells of the same species. Consequently, a microbial population can now be studied as a heterogeneous group of physiologically distinct individuals. Moreover, the major contribution of less abundant but highly active microorganisms to ammonium and carbon uptake underlines the great importance of rare keystone species to the nitrogen and carbon cycles in the environment. The HISH-SIMS method opens new lines of research in environmental microbiology, especially by enabling studies of the ecophysiology of individual, phylogenetically identified cells and by the capacity to track not only the flows of nitrogen and carbon but also those of phosphorus, sulfur, and other biologically active elements within microbial communities.

## Materials and Methods

**Measurements of Physicochemical Parameters.** Temperature, conductivity, dissolved oxygen, turbidity, and redox potential were measured at depth intervals of 1 m by a pumpcast conductivity-temperature-depth system equipped with an oxygen sensor (17). Nutrients were analyzed at the same depth intervals using standard methods (*SI Text*).

**Culture Preparation and Fixation.** *E. coli* strain DSM 30083 and *Azoarcus* sp. strain HxN1 were grown as described (*SI Text*). Cells were prepared for hybridization using standard protocols (*SI Text*).

**Sample Collection and Preparation.** Water samples were collected from the center of Lake Cadagno (46° 33′ N, 8° 43′ E) in June 2007. The depth at the center (the deepest point) was 21 m. Water samples were collected at depths of 10.5, 11.5, and 12.5 m, fixed for FISH in 1% PFA for 1 h at room temperature, filtered on polycarbonate filters, and kept at −20 °C until processing. Parallel water samples from 11.5-m depth were collected and incubated with $^{15}$N-labeled ammonium (21.6 atom percent $^{15}$N) and $^{13}$C-labeled bicarbonate (19.3 atom percent $^{13}$C) in 250-mL bottles at in situ light and temperature conditions for 4, 8, and 12 h (*SI Text*). Subsamples were taken for bulk measurements of nitrogen and carbon and for nanoSIMS analysis of single cells (see *SI Text*).

**Whole Cell Hybridization.** Catalyzed reporter deposition (CARD)-FISH and cell counts were done using standard protocols (*SI Text*). The oligonucleotide probes used in this study are shown in Table S3.

For nanoSIMS analysis, fixed cells were permeabilized in a lysozyme solution [10 mg mL$^{-1}$ in 0.05 M EDTA (pH 8.0) and 0.1 M Tris·HCl, pH (7.5); Fluka] for 1 h at 37 °C. After permeabilization, filters were washed twice with 2 mL of ultrapure
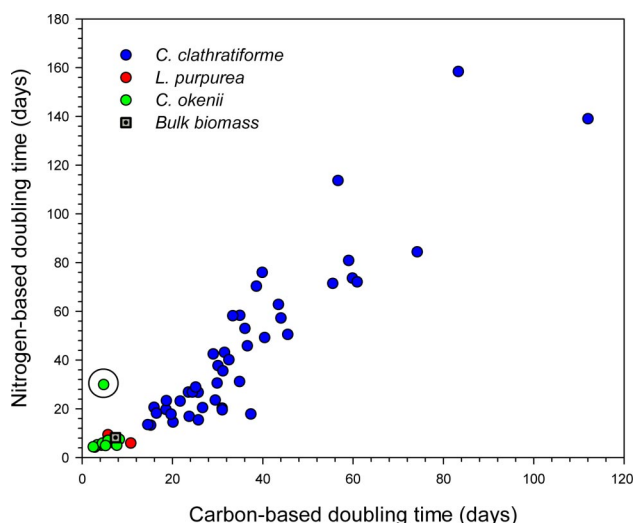


**Fig. 7.** Nitrogen- and carbon-based doubling times calculated for bulk biomass and individual *C. clathratiforme*, *L. purpurea*, and *C. okenii* cells. The doubling times were calculated using the $^{15}$N/$^{14}$N and $^{13}$C/$^{12}$C ratios and assuming that all carbon and nitrogen assimilated were channeled into growth.

water (MQ; Millipore), treated with HCl (0.01 M) for 10 min, washed twice in MQ water, and dehydrated with 96% ethanol for 1 min. Before hybridization, filters were prehybridized for 1 h at 46 °C in hybridization buffer containing 0.9 M NaCl, 40 mM Tris-HCl (pH 7.5), 10% dextran sulfate, 0.01% SDS (SDS), 10% Blocking Reagent (Boehringer), $1\times$ Denhard's reagent, 0.26 mg mL$^{-1}$ sheared salmon sperm DNA (Ambion), 0.2 mg mL$^{-1}$ yeast RNA (Ambion), and the corresponding formamide concentration (Table S3). The hybridization was performed using the protocol previously described (41) with the following modifications: After pre-hybridization, the HRP-labeled probe working solution (50 ng $\mu$L$^{-1}$; Biomers) was added (1:150 vol/vol) to the hybridization buffer and well mixed. Hybridizations were carried out for 6 h at 46 °C. After hybridization, filters were incubated in 50 mL of prewarmed washing buffer containing NaCl (215 mM for Chlc190, 46 mM for Apur453, and 70 mM for Cmok453 hybridized filters), 5 mM EDTA (pH 8.0), 20 mM Tris-HCl (pH 7.5), and 0.01% SDS for 15 min at 48 °C. After washing, filters were transferred in $1\times$ PBS (pH 7.6) for 30 min to equilibrate the probe-delivered HRP. Subsequently, the filters were incubated for 20 min at 46 °C in darkness for tyramide signal amplification. The reactant mixture contained amplification buffer and fluorine-containing tyramides (1,000:1 vol/vol) and 0.015% H$_2$O$_2$. The filters were then washed once for 15 min in $1\times$ PBS in darkness, twice with MQ water, and once for 1 min in 96% ethanol. Synthesis of tyramides and preparation of the substrate mixture containing amplification buffer and H$_2$O$_2$ were done as described (*SI Text* and ref. 42).

**Nitrogen and Carbon Bulk Measurements.** Abundances of $^{15}$N and $^{13}$C were measured using standard methods (*SI Text*).

**NanoSIMS Analysis of Single Cells—Image Acquisition and Data Processing.** The hybridized filters were analyzed between January 2007 and October 2007 using a NanoSIMS 50 and a NanoSIMS 50L manufactured by Cameca. For each individual cell, we recorded simultaneously secondary ion images of $^{12}$C$^-$, $^{13}$C$^-$, $^{12}$C$^{14}$N$^-$, $^{12}$C$^{15}$N$^-$, and $^{19}$F$^-$ using 5 electron multipliers (Figs. 3–5). Measurements were performed using 3 sets of analytical conditions (see *SI Text*). The $^{12}$C$^-$, $^{13}$C$^-$, $^{19}$F$^-$, $^{12}$C$^{14}$N$^-$, and $^{12}$C$^{15}$N$^-$ ions were collected and measured in parallel at a mass resolution sufficient to separate the $^{13}$C$^-$ from the $^{12}$CH$^-$ and $^{12}$C$^{15}$N$^-$ from the $^{13}$C$^{14}$N$^-$. Images and data were processed using the proprietary CAMECA Win-Image processing software working under PC Windows XP environment (see *SI Text*).

**Biovolume Calculation and Biomass Conversion.** The sizes of *C. okenii*, *L. purpurea*, and *C. clathratiforme* cells were directly measured from the epifluorescence microscope images taken after fluorescence in situ hybridization and DAPI staining. Biovolume calculation and biomass conversion are described in *SI Text*.

**Calculation of the Ammonium and Inorganic Carbon Assimilation Rates.** Amounts of ammonium and inorganic carbon assimilated by individual cells were calculated from the $^{15}$N/$^{14}$N and the $^{13}$C/$^{12}$C ratios of the individual regions of interest (Table S2), the mean biovolume for the corresponding species, and the amounts of label added in the incubation experiments. The total assimilation for each species was calculated by multiplying the average assimilation rates of individual cells by the number of cells of the corresponding species (as determined by FISH).

**Calculation of the Doubling Times.** Doubling times of the 3 species were calculated using the $^{15}$N/$^{14}$N and $^{13}$C/$^{12}$C ratios, the biovolume and the conversion factor into biomass to calculate first the $^{15}$N and $^{13}$C excess (as atomic percent) into individual cells. Using these values and the percentage of label added in the incubation experiments as well as the time of incubation, we calculated the doubling time for individual *C. okenii*, *C. clathratiforme*, and *L. purpurea* cells.

**SI.** Further information, including Figs. S2 and S3, is available in *SI Text*.

1. Joyce EA, Chan K, Salama NR, Falkow S (2002) Redefining bacterial populations: A post-genomic reformation. *Nat Rev Genet* 3:462–473.
2. Rappe MS, Giovannoni SJ (2003) The uncultured microbial majority. *Annu Rev Microbiol* 57:369–394.
3. Acinas SG, *et al.* (2004) Fine-scale phylogenetic architecture of a complex bacterial community. *Nature* 430:551–554.
4. DeLong EF (2002) Microbial population genomics and ecology. *Curr Opin Microbiol* 5:520–524.
5. DeLong EF (2004) Microbial population genomics and ecology: The road ahead. *Environmental Microbiology* 6:875–878.
6. Orphan VJ, House CH, Hinrichs KU, McKeegan KD, DeLong EF (2001) Methane-consuming archaea revealed by directly coupled isotopic and phylogenetic analysis. *Science* 293:484–487.
7. Neufeld JD, Wagner M, Murrell JC (2007) Who eats what, where and when? Isotope-labelling experiments are coming of age. *ISME Journal* 1:103–110.
8. Cliff JB, Gaspar DJ, Bottomley PJ, Myrold DD (2002) Exploration of inorganic C and N assimilation by soil microbes with time-of-flight secondary ion mass spectrometry. *Appl Environ Microbiol* 68:4067–4073.
9. Lechene C, *et al.* (2006) High-resolution quantitative imaging of mammalian and bacterial cells using stable isotope mass spectrometry. *Journal of Biology* 5:20.
10. Popa R, *et al.* (2007) Carbon and nitrogen fixation and metabolite exchange in and between individual cells of Anabaena oscillarioides. *ISME J* 1:354–360.
11. Lechene CP, Luyten Y, McMahon G, Distel DL (2007) Quantitative imaging of nitrogen fixation by individual bacteria within animal cells. *Science* 317:1563–1566.
12. Kuypers MMM, Jorgensen BB (2007) The future of single-cell environmental microbiology. *Environmental Microbiology* 9:6–7.
13. Li T, *et al.* (2008) Simultaneous analysis of microbial identity and function using NanoSIMS. *Environmental Microbiology* 10:580–588.
14. Del Don C, Hanselmann KW, Peduzzi R, Bachofen R (2001) The meromictic alpine Lake Cadagno: Orographical and biogeochemical description. *Aquat Sci* 63:70–90.
15. Tonolla M, Demarta A, Peduzzi R, Hahn D (1999) In situ analysis of Phototrophic sulfur bacteria in the chemocline of meromictic Lake Cadagno (Switzerland). *Appl Environ Microbiol* 65:1325–1330.
16. Tonolla M, Peduzzi S, Demarta A, Peduzzi R, Hahn D (2004) Phototropic sulfur and sulfate-reducing bacteria in the chemocline of meromictic Lake Cadagno, Switzerland. *J Limnol* 63:161–170.
17. Tonolla M, Peduzzi R, Hahn D (2005) Long-term population dynamics of phototrophic sulfur bacteria in the chemocline of Lake Cadagno, Switzerland. *Appl Environ Microbiol* 71:3544–3550.
18. Overmann J (2006) The family Chlorobiaceae. *The Prokaryotes*, eds Dworking M, Falkow S, Rosenberg E, Schleifer K-H, Stackebrandt E (Springer, New York), Vol 7, pp 359–378.
19. Imhoff JF (2006) The Chromatiaceae. *The Prokaryotes*, eds Dworking M, Falkow S, Rosenberg E, Schleifer K-H, Stackebrandt E (Springer, New York), Vol 6, pp 846–873.
20. Van Gemerden H, Mas J (1995) Ecology of phototrophic sulfur bacteria. *Anoxygenic Photosynthetic Bacteria*, eds Blankenship RE, Madigan MT, Bauer CE (Kluwer Academic Publishers, Dordrecht/Boston/London), pp 49–85.
21. Bossard P, *et al.* (2001) Limnological description of the Lakes Zurich, Lucerne, and Cadagno. *Aquat Sci* 63:225–249.
22. Tonolla M, Peduzzi S, Hahn D, Peduzzi R (2003) Spatio-temporal distribution of phototrophic sulfur bacteria in the chemocline of meromictic Lake Cadagno (Switzerland). *FEMS Microbiol Ecol* 43:89–98.
23. Guerrero R, *et al.* (1986) Predatory prokaryotes—Predation and primary consumption evolved in bacteria. *Proc Natl Acad Sci USA* 83:2138–2142.
24. Clarke KJ, Finlay BJ, Vicente E, Llorens H, Miracle MR (1993) The complex life-cycle of a polymorphic prokaryote epibiont of the photosynthetic bacterium chromatium-weissei. *Arch Microbiol* 159:498–505.
25. Redfield A, Ketchum B, Richards F (1963) The influence of organisms on the composition of sea-water. *The Sea*, ed Hill M (Interscience, New York), pp 26–77.
26. Del Don C, Hanselmann KW, Peduzzi R, Bachofen R (1994) Biomass composition and methods for the determination of metabolic reserve polymers in phototrophic sulfur bacteria. *Aquat Sci* 56:1–15.
27. Schmidt GL, Kamen MD (1970) Variable cellular composition of Chromatium in growing cultures. *Arch Mikrobiol* 73:1–18.
28. Eichler B, Pfennig N (1988) A new purple sulfur bacterium from stratified fresh-water lakes, Amoebobacter-Purpureus Sp-Nov. *Arch Microbiol* 149:395–400.
29. Overmann J, Pfennig N (1989) Pelodictyon-Phaeoclathratiforme Sp-Nov, a new brown-colored member of the Chlorobiaceae forming net-like colonies. *Arch Microbiol* 152:401–406.
30. Folt CL, Wevers MJ, Yoder-Williams MP, Howmiller RP (1989) Field study comparing growth and viability of a population of phototrophic bacteria. *Appl Environ Microbiol* 55:78–85.
31. Schanz F, Fischer-Romero C, Bachofen R (1998) Photosynthetic production and photoadaptation of phototrophic sulfur bacteria in Lake Cadagno (Switzerland). *Limnology and Oceanography* 43:1262–1269.
32. Fenchel T, Finlay BJ (1990) Anaerobic free-living protozoa—Growth efficiencies and the structure of anaerobic communities. *FEMS Microbiol Ecol* 74:269–275.
33. Güde H (1989) The role of grazing on bacteria on plankton succession. *Plankton Ecology: Succession in Plankton Communities*, ed Sommer U (Springer Verlag, New York), pp 337–364.
34. Hahn MW, Hofle MG (2001) Grazing of protozoa and its effect on populations of aquatic bacteria. *FEMS Microbiol Ecol* 35:113–121.
35. Moore LR, Rocap G, Chisholm SW (1998) Physiology and molecular phylogeny of coexisting Prochlorococcus ecotypes. *Nature* 393:464–467.
36. Jaspers E, Overmann J (2004) Ecological significance of microdiversity: Identical 16S rRNA gene sequences can be found in bacteria with highly divergent genomes and ecophysiologies. *Appl Environ Microbiol* 70:4831–4839.
37. Thompson JR, *et al.* (2005) Genotypic diversity within a natural coastal bacterioplankton population. *Science* 307:1311–1313.
38. Beja O, *et al.* (2002) Comparative genomic analysis of archaeal genotypic variants in a single population and in two different oceanic provinces. *Appl Environ Microbiol* 68:335–345.
39. Tolker-Nielsen T, Holmstrom K, Boe L, Molin S (1998) Non-genetic population heterogeneity studied by in situ polymerase chain reaction. *Mol Microbiol* 27:1099–1105.
40. Pernthaler A, Amann R (2004) Simultaneous fluorescence in situ hybridization of mRNA and rRNA in environmental bacteria. *Appl Environ Microbiol* 70:5526–5533.
41. Pernthaler A, Pernthaler J, Amann R (2002) Fluorescence in situ hybridization and catalyzed reporter deposition for the identification of marine bacteria. *Appl Environ Microbiol* 68:3094–3101.
42. Pernthaler A, Pernthaler J, Amann J (2004) Sensitive multi-color fluorescence in situ hybridization for the identification of environmental microorganisms. *Molecular Microbial Ecology Manual*, eds Kowalchuk GA, de Bruijn FJ, Head IM, Akkermans ADL, van Elsas JD (Kluwer Academic Publishers, Dordrecht/Boston/London), pp 711–726.